

## Article

# Inactivation of *Escherichia coli* Using Biogenic Silver Nanoparticles and Ultraviolet (UV) Radiation in Water Disinfection Processes

Ljubica Tasic<sup>1,\*</sup>, Danijela Stanisic<sup>1</sup>, Caio H. N. Barros<sup>1,2</sup>, Leticia Khater Covesi<sup>1</sup> and Erick R. Bandala<sup>3,\*</sup>

<sup>1</sup> Laboratory of Biological Chemistry, Department of Organic Chemistry, Institute of Chemistry, University of Campinas (UNICAMP), P.O. Box 5147, Campinas 13083-970, Brazil; dacici.stanisic@gmail.com (D.S.); caio.henrique@nibr.ie (C.H.N.B.); leticia@i9pi.com.br (L.K.C.)

<sup>2</sup> National Institute for Bioprocessing Research and Training (NIBRT), A94 X099 Dublin, Ireland

<sup>3</sup> Division of Hydrologic Sciences, Desert Research Institute, 775 E. Flamingo Road, Las Vegas, NV 89119, USA

\* Correspondence: ljubica@unicamp.br (L.T.); erick.bandala@dri.edu (E.R.B.); Tel.: +1-702-862-5395 (E.R.B.)

**Abstract:** This work tested the antimicrobial activity of three different biogenic silver nanoparticles (AgNPs) against *Escherichia coli* (*E. coli*) for water disinfection processes. The influence of different AgNP capping or stabilizing agents (e.g., protein or carbohydrate capped) and the use of ultraviolet (UV) radiation on the disinfection process were also assessed. The use of UV radiation was found to enhance the antimicrobial effects of AgNPs on *E. coli*. The antibacterial effects of AgNPs depended on the type of the capping biomolecules. Protein-capped nanoparticles showed greater antimicrobial effects compared with carbohydrate-capped (cellulose nanofibers, CNF) nanoparticles. Those capped with the fungal secretome proteins were the most active in *E. coli* inactivation. The least *E. coli* inactivation was observed for CNF-capped AgNPs. The size of the tested AgNPs also showed an expected effect on their anti-*E. coli* activity, with the smallest particles being the most active. The antimicrobial effects of biogenic AgNPs on *E. coli* make them an effective, innovative, and eco-friendly alternative for water disinfection processes, which supports further research into their use in developing sustainable water treatment processes.

**Keywords:** biogenic nanomaterials; inactivation; *Escherichia coli*; silver nanoparticles; water disinfection



**Citation:** Tasic, L.; Stanisic, D.; Barros, C.H.N.; Covesi, L.K.; Bandala, E.R. Inactivation of *Escherichia coli* Using Biogenic Silver Nanoparticles and Ultraviolet (UV) Radiation in Water Disinfection Processes. *Catalysts* **2022**, *12*, 430. <https://doi.org/10.3390/catal12040430>

Academic Editors: Aida M. Diez and Vitor J. P. Vilar

Received: 28 February 2022

Accepted: 8 April 2022

Published: 11 April 2022

**Publisher's Note:** MDPI stays neutral with regard to jurisdictional claims in published maps and institutional affiliations.



**Copyright:** © 2022 by the authors. Licensee MDPI, Basel, Switzerland. This article is an open access article distributed under the terms and conditions of the Creative Commons Attribution (CC BY) license (<https://creativecommons.org/licenses/by/4.0/>).

## 1. Introduction

Over the last decade, improving access to safe drinking water through developments in science and technology has been determined to be the most suitable way to direct efforts for increasing water supplies and face the expected increase in water-related problems [1]. The challenge is significant because it calls for more research aimed at identifying innovative methods that can improve water quality with the lowest environmental footprint.

In the last few years, using greener procedures to synthesize nanomaterials (NMs) to minimize the environmental impacts of treatment processes has become a significant scientific task [2]. Microorganisms and plant biomass have gained popularity as eco-friendly materials that can be used to synthesize nanocomposites and nanoparticles for water treatment [3]. Biogenic silver nanoparticles (AgNPs) in particular have emerged as interesting antimicrobial NMs. These NMs have been widely reported to reduce infections during burn treatment, prevent bacterial growth in medical equipment and water treatment [4–6], and produce a significant increase in antimicrobial activity compared with chemically produced AgNPs [7].

Our research group previously reported the synthesis of biogenic AgNPs using sources such as sweet orange (*Citrus sinensis*) peel extract [3] and a fungal (*Fusarium oxysporum*) filtrate solution [8], and their antimicrobial activity against *Xanthomonas axonopodis* pv. *citri* and *Candida parapsilosis*. Despite the significance of medical and agricultural applications

for the biogenic AgNPs, another highly significant potential use for these materials is water disinfection. Waterborne diseases related to a lack of access to safe drinking water are a major threat to millions of people around the world. Therefore, developing innovative water treatment processes is paramount in achieving the United Nations' Sustainable Development Goals, because reduced precipitation and changes in rain patterns are expected to affect existing and emerging pathogens and increase the incidence of microbial diseases [9]. Water disinfection using the photocatalytic activity of biogenic AgNPs has previously been reported to be an effective method for inactivating *Escherichia coli* (*E. coli*) bacteria, which involves generating superoxide radicals and inactivating up to 7.0 log cells within 60 min using visible or ultraviolet (UV) radiation [10,11].

The goals of this work were to study the antimicrobial effects of three different biogenic AgNPs on *E. coli* in water disinfection processes, to assess the effect of the AgNP load, and to evaluate the influence of the synthesis procedure and the use of ultraviolet (UV) radiation source on the disinfection process.

## 2. Results and Discussion

### 2.1. Biogenic AgNP Characterization

The AgNP-FU nanoparticles were shown to be spherical in form with sizes of  $28.0 \pm 13.1$  nm and a polydispersity value of 0.231. Their zeta potential was  $-31.7 \pm 2.8$  mV and those were found to be stable for one year. AgNP-OR also showed spherical forms with sizes of  $48.1 \pm 20.5$  nm, a polydispersity value of 0.312, and zeta potential of  $-19.0 \pm 0.4$  mV. The third type of studied particle AgNP Hsp-CNF exhibited spherical forms, sizes of  $25.4 \pm 12.5$  nm, and a polydispersity of 0.314. Their zeta potential was  $-28.2 \pm 1.0$  mV and those were stable for one year. Figure 1 shows TEM images of the biogenic AgNPs synthesized and stabilized by *Fusarium oxysporum* filtrate (AgNP-FU), orange peel extract (AgNP-OR), and hesperidin and cellulose nanofibers (AgNP Hsp-CNF). It is worth noting that all NPs presented spherical forms and core-shell morphology, with a metallic silver ( $\text{Ag}^0$ ) core and a shell, shown as a lighter gray capping observable in TEM images, formed either by proteins or CNF [12] capping. The observed polydispersity of the nanoparticles was also consistent with the physical measurements obtained in their characterization. These results are in agreement with those from studies in which biogenic AgNPs were produced using biochemical sources. For example, another study used two fungi (*Rhodotorula glutinis* and *Rhodotorula mucilaginosa*) in the production of AgNPs [13]. These authors found that the biogenic AgNPs had a diameter in the 30 nm to 50 nm range and the protein-capped layer including the metallic  $\text{Ag}^0$  core was 21–24 nm thick, which is within the same order of magnitude as the NPs reported here. In a different study, fruit peels were used to synthesize AgNPs within the particle size range between 8 nm and 25 nm [14]. The AgNPs were found to have protein-capped layers and a zeta potential ranging from  $-11.4$  to  $-20$  mV, both values were the same order of magnitude found in our study. Other authors used dialdehyde cellulose as a reducing and stabilizing agent for the synthesis of AgNPs [15]. They found the formation of spherical AgNPs with an average size of 30 nm and zeta potential values ranging from  $-27.5$  mV to  $-39.1$  mV. Both values were within the same order of magnitude found for our NPs attached to the cellulose nanocrystal surfaces. As mentioned before, we were unable to observe the distribution of the AgNPs along the cellulose fibers.

In their study, Xu et al. [15] suggested that the cellulose nanocrystals aspect ratio and specific surface provided support for AgNPs and prevented aggregation. Unfortunately, they did not report the actual size of the cellulose nanocrystals used, and therefore it was not possible to compare them with the fibers used in our study. Finally, Abdel-Raouf et al. [16] used marine alga extracts to produce AgNPs, which showed high stability and particle sizes in the 50 nm to 86 nm range. They suggested a mechanism for reducing silver ions by the hydroxyl groups and acid groups present in the algal extracts used. We anticipate that something similar could happen during the biogenic production of AgNPs using

the different processes described here, but more detailed research is needed to prove this theory.

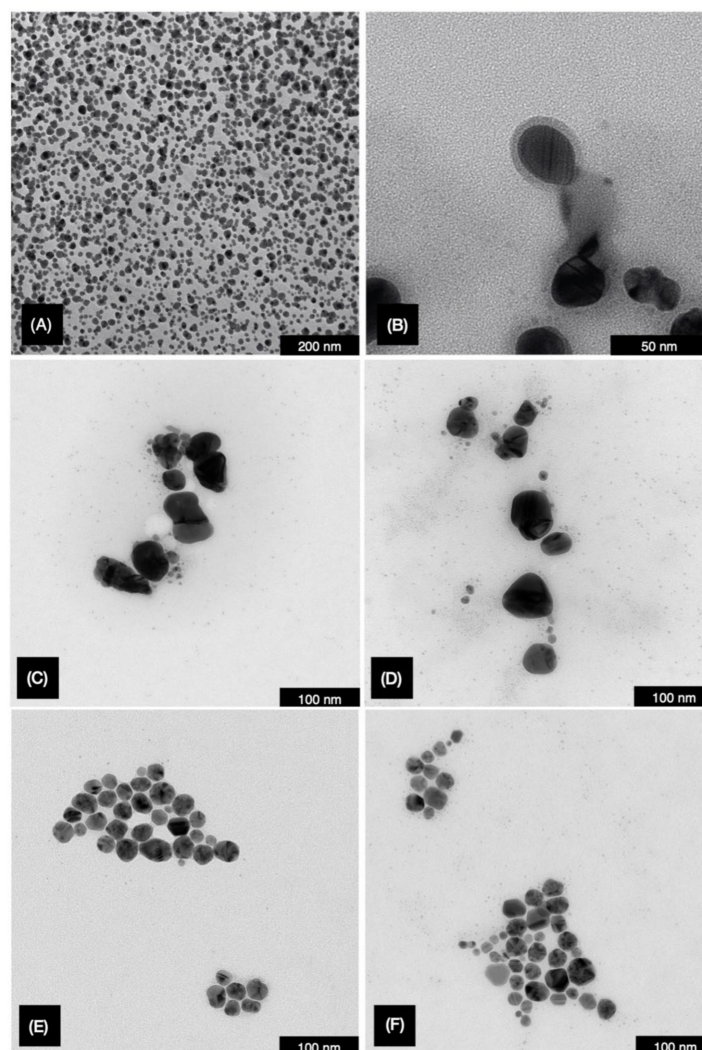


**Figure 1.** The TEM images of the different biogenic AgNPs synthesized and stabilized with *Fusarium oxysporum* proteins (AgNP-FU), (A,B), orange peel water extract (AgNP-OR), (C,D), and hesperidin and cellulose nanofibers (AgNP Hsp-CNF), (E,F) (images were adapted from the literature [3,8]).

## 2.2. *E. coli* Inactivation Tests

Three types of AgNPs were used to study the capabilities of AgNPs to inactivate *E. coli* and their synergistic effects with UV radiation. Figure 2a shows the inactivation curves for AgNP Hsp-CNF with and without UV radiation, as well as the effects of UV radiation alone. As shown, low inactivation was observed when using the AgNP Hsp-CNF alone or combined with UV radiation (Figure 2). These results were in opposition to results reported by Phan et al. [17], who reported significant bactericidal activity of cellulose nanofibers decorated with silver nanoparticles. However, the authors used silver nanoparticles impregnated into cellulosic fibers as a functional composite material, and UV radiation as a reducing agent, which is a completely different approach than the one used herein. Wahab et al. [18] also reported the use of cellulose acetate nanofibers embedded with AgNPs anchored to TiO<sub>2</sub> nanoparticles for antibacterial applications. One significant difference between the AgNPs reported in those studies and the nanoparticles reported here is the particle size [18]. The average size of AgNP Hsp-CNF was 25 nm, whereas the particles reported with high antibacterial applications had a particle size less than 10 nm.

Figure 2b shows the inactivation curves when using AgNP-OR. As shown, AgNP-OR had some bacterial inactivation only when combined with UV irradiation, but no or very low inactivation effects were observed in trials without UV irradiation (Figures 2 and 3).

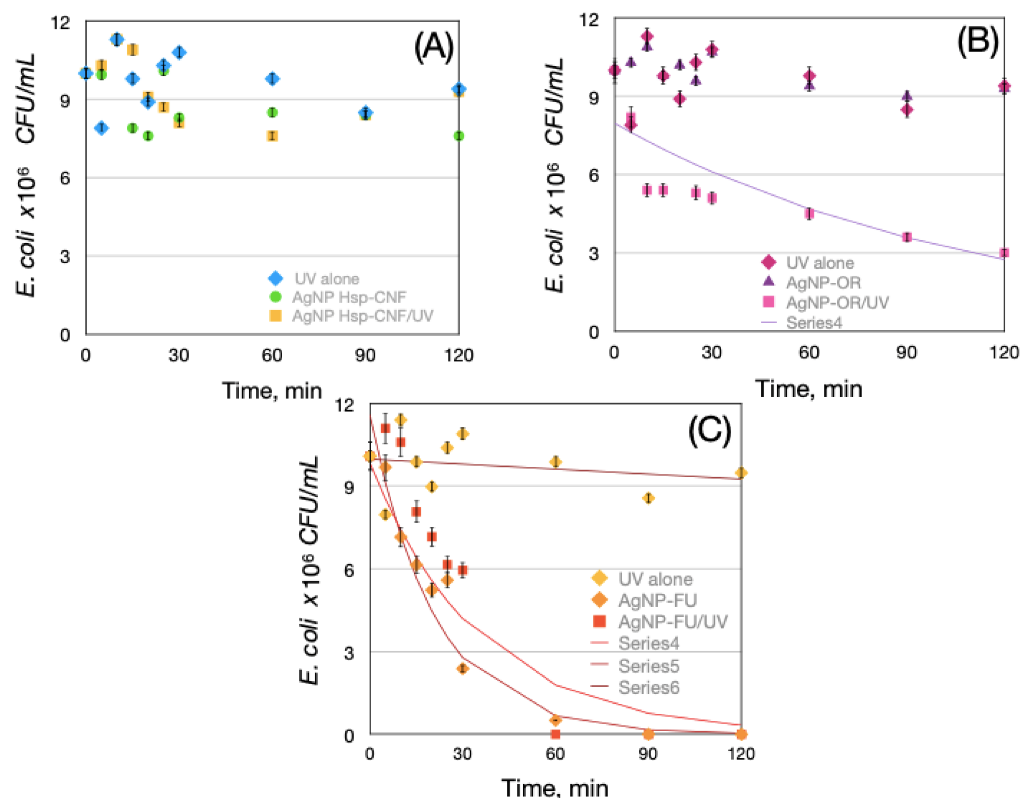


**Figure 2.** *E. coli* inactivation with UV radiation expressed as remaining CFU/mL over time using silver nanoparticles obtained using bio-based synthesis. (A) AgNP Hsp-CNF, hesperidin (isolated from orange peels) and stabilized with cellulose nanofibers; (B) AgNP-OR, orange peels water extract; and (C) AgNP-FU, fungal filtrate water extract. Graphs show UV alone (364 nm), and in joint action with AgNPs.

Nano-sized  $\text{Ag}^0$  particles have been reported with the ability to bind the bacterial cell DNA, halting cell replication machinery which has been widely demonstrated by the production of inhibition zones using the agar well diffusion method [19]. In the case of AgNP-OR almost no effect on *E. coli* was observed for the NPs alone suggesting the reported mechanism does not occur in the process. Photocatalytic activity of biogenic AgNPs has been reported in the past besides the antimicrobial activity usually found [20]. These authors suggested that the photocatalytic activity of biogenic AgNPs is related to the generation of charge carriers, as previously suggested for other semiconductors [21–23]. This mechanism could be also involved in the results reported here, but more detailed research is required to prove this hypothesis.

Figure 2B shows the inactivation curves obtained using AgNP-OR, which were capable of inactivating *E. coli* in a similar way when compared to UV radiation (Figure 3). The *E. coli* inactivation was enhanced when UV radiation was used together with AgNP-OR in the reaction mixture (Figures 2B and 3).

The trend showed that *E. coli* inactivation effects could be related to the size, coating agent, and zeta potential of nanoparticles. For example, AgNP-FU showed a medium particle size (28 nm), which is comparable to AgNP Hsp-CNF (25.4 nm). Nevertheless, AgNP-FU showed the highest inactivation activity, whereas AgNP Hsp-CNF showed very low activity (Figures 2 and 3).

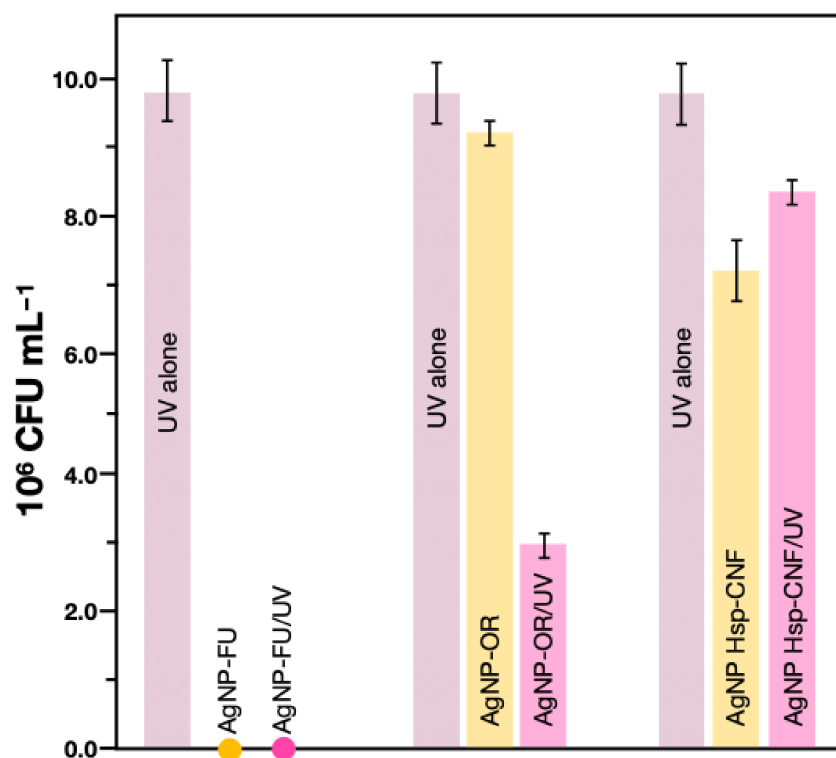


**Figure 3.** Colony-forming units (CFU × 10<sup>6</sup> per mL) of existing *E. coli* after exposure to UV radiation for 2 h and/or three biogenic AgNPs.

Thatikayala et al. [24] suggested that the antibacterial activity of biogenic AgNPs could be related to size, dispersion, and spherical morphology, which are usually associated with a larger surface area that allows higher interaction with bacteria. In this case, particle size is not significantly different between AgNP-FU and AgNP Hsp-CNF, but their inactivation activities are completely different. The nature of the phytochemicals that protect nanoparticles has also been related to the increase in antibacterial effects [25].

The nature of the different coatings and small physical-chemical differences among the tested AgNPs probably caused their different effects on *E. coli*. For example, AgNP-FU showed a polydispersity of 0.23 and a zeta potential of −31.7 mV, which means that those particles had the sharpest molecular weight distribution of the entire materials set and formed the most stable colloidal dispersion. The dispersion of AgNP-FU may be the key to their higher inactivation capability because it may allow a higher interaction between the bacteria and nanoparticles. On the other hand, AgNP Hsp-CNF showed a smaller particle size, higher polydispersity (0.314), and higher zeta potential values than AgNP-FU, which means a broader size distribution and lower colloidal stability. Finally, AgNP-OR showed a greater size (e.g., 48.0 nm) and a polydispersity similar to AgNP Hsp-CNF, but the lowest colloidal stability due to the lowest zeta potential (−19 mV). Nevertheless, physical differences among the investigated silver nanoparticles are insufficient to justify the differences in their bioactivities with *E. coli*. Therefore, these differences must be considered along with the chemical differences in their coatings.

The performance of the AgNP-OR/UV, AgNP-FU, and AgNP-FU/UV processes for *E. coli* inactivation was found to be significantly higher than the results from other studies. For example, Raota et al. [26] reported a 47% reduction of the *E. coli* bacterial count using biogenic AgNPs prepared using Ives cultivar (*Vitis labrusca*) extract. In our study, over 2-log cycles (99.0% inactivation) were achieved for the AgNP-OR/UV, and over 4-log cycles (99.99% inactivation) were achieved using either AgNP-FU or AgNP-FU/UV after 120 min of reaction. In another study using magnetic Ag/Fe, N-TiO<sub>2</sub>/Fe<sub>3</sub>O<sub>4</sub> (AgFeNTFS), He et al. [27] found a 6.4-log reduction in cell density of *E. coli* after 120 min of visible

radiation, which is slightly higher than our results, but they used a more complex material composite created with conventional chemical synthetic methods.

To fairly compare the performance of the different materials reported here against other studies, the experimental data were fitted using Chick's law, which is a pseudo-first-order kinetic model with respect to the residual cell concentration that assumes an excess of disinfectant in the inactivation reaction [28]. Table 1 and Figure 4 show the results of fitting the experimental data to Chick's law. As shown, Chick's law fit the experimental results fairly well under conditions in which bacteria inactivation was achieved by generating a correlation coefficient ( $R^2$ ) as high as 0.87 in the worst case (e.g., AgNP-OR/UV).

**Table 1.** Results of fitting the experimental antibacterial data to Chick's law, in which the inactivation rate value,  $k$ , is shown.

Disinfection Process	$k$ , $\text{min}^{-1}$ ( $R^2$ )
AgNP-OR/UV	0.0089 (0.87)
AgNP-FU	0.028 (0.92)
AgNP-FU/UV	0.047 (0.94)

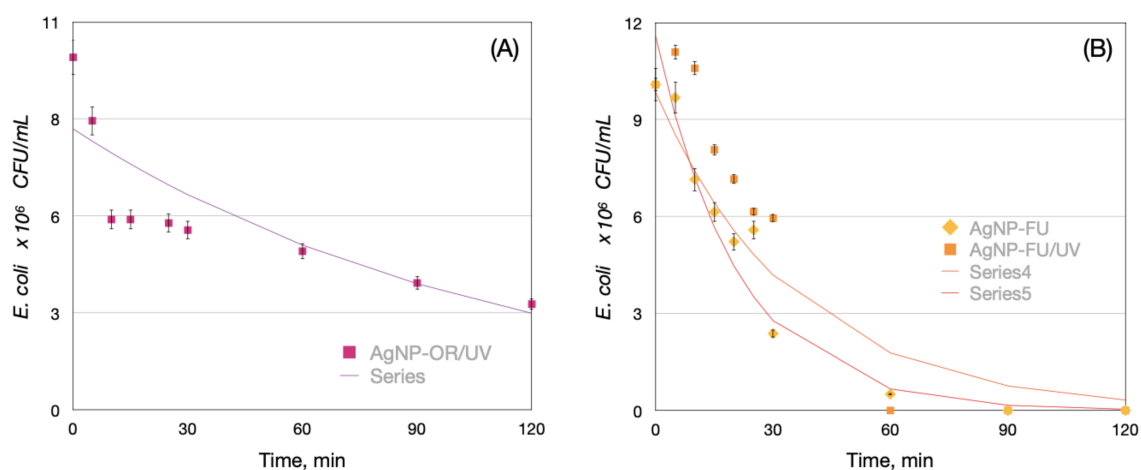


**Figure 4.** Simulation of the experimental results using Chick's law model for two types of silver nanoparticles used in *E. coli* disinfection: (A) AgNP-OR with UV light, and (B) AgNP-FU and AgNP-FU with UV light.

Based on the overall results, the AgNP-OR/UV process generated the lowest inactivation rate value (e.g.,  $0.0089 \text{ min}^{-1}$  compared with AgNP-FU and AgNP-FU/UV, which had inactivation rate values more than three- and fivefold, respectively, the value estimated for AgNP-OR/UV (Table 1). However, the inactivation rate estimated for the worst reaction conditions ( $0.0089 \text{ min}^{-1}$ ) was only slightly lower than values reported in another UV photocatalytic disinfection study using Ag@TiO<sub>2</sub> nanoparticles (Sreeja and Vidya Shetty, 2016) [28].

These authors found inactivation rate values as high as  $0.016 \text{ min}^{-1}$  using Ag@TiO<sub>2</sub> at loads as high as  $100 \text{ g L}^{-1}$ , which was three orders of magnitude greater than the AgNP load used in this study. Sreeja and Vidya Shetty (2016) [28] also reported an inactivation rate value as high as  $0.127 \text{ min}^{-1}$  using  $1 \text{ g L}^{-1}$  of Ag@TiO<sub>2</sub> nanoparticles. This result is more than twofold greater than the highest inactivation rate achieved for AgNP-FU/UV in this work, but that study used a nanoparticle load that was four orders of magnitude greater than the load used in this study.

The Chick's law model was also used to simulate experimental results and the resulting curves are included as lines in Figure 4. As shown, Chick's law model fit the experimental results fairly well, and therefore served as a good predictive model for the inactivation curve behavior.

### 2.3. Assessing the Effects of AgNP-Capping Agents

Silver nanoparticles (AgNPs) obtained using biogenic processes have interesting physicochemical properties and significant antimicrobial activity. In general, AgNPs obtained herein and through different synthetic strategies differ in size (varying from 20 nm to 40 nm), and are considered medium-size nanoparticles, zeta potential (usually negative), and capping agents (e.g., proteins, polymers, and other molecules), as well as a broad range of molecular masses and chemical groups that are usually tightly interacting with a silver(0), and adhered onto silver(0) or to each other, forming the second capping layer, by physical-chemical interactions. Different methods for AgNP synthesis can be optimized and designed to tailor capping agents and enhance their antibacterial and antiviral activities [29]. Uncapped AgNPs were found to have no antibacterial activity in the presence of serum proteins because of their interaction with bovine serum albumin (BSA), whereas the protein-capped AgNPs showed no interaction with BSA, which enabled their greater uptake and intracellular load and promoted more extensive bacterial death.

The three biogenic AgNPs were compared to verify whether they exhibited similar effects on *E. coli* and to determine if these effects could be correlated with the properties of the tested AgNPs and their capping agents. Fungal secretome and orange extract proteins linked to the corresponding AgNPs were digested with trypsin and the tryptic peptides were subjected to UPLC-MS/MS analyses. The MASCOT server was used to identify the proteins using data banks. Several proteins from the fungal secretome and orange extract, which were published previously [3] in the case of orange extract proteins, were identified using this method, and they are listed in Table S1 in the Supplementary Material [3,8]. For more details on the targeted proteomic mass spectrometry analysis, see Ballottin et al. [8]. The AgNP Hsp-CNF obtained using the bio-based method just had the cellulose nanofiber coating, and were not capped with proteins.

Table S1 (Supplementary Material) lists 22 proteins linked to the AgNP-FU and 27 proteins linked to the AgNP-OR identified according to the NCBI database. Five proteins from the *Fusarium oxysporum* secretome were identified as hypothetical proteins. Out of the identified proteins, enzymes such as dehydrogenases, malate dehydrogenase, NAD(P)<sup>+</sup>-glutamate dehydrogenases, and 6-phosphogluconate dehydrogenase were involved in AgNP-FU capping, as well as some hypothetical proteins: FG02461.1 and LOC100191904, which are also NAD(P)<sup>+</sup>-dependent redox enzymes. This superfamily includes a wide variety of protein families, such as dehydrogenases, oxidoreductases, synthases, and others. For example, two proteins from the family of dehydrogenases: glutamate dehydrogenase and malate dehydrogenase are fundamental in fungal metabolism as well as nitrogen and carbon absorption [8]. Other identified enzymes from AgNP-FU are known to play specific roles in metabolic pathways involving protein hydrolysis (catabolic) and amino acid importation, as well as carbohydrate catabolic pathways, which contribute to fungal growth.

The protein-rich capping of AgNP-OR was already identified by the NCBI database, including seven hypothetical and five uncharacterized proteins from *Citrus sinensis*. All of them are expected to adhere to AgNP-OR through cysteine residues and amino groups in their side chains, which corroborates that sulfur and nitrogen atoms can interact with the surface of silver(0), which has been suggested previously [12]. Therefore, the protein coatings on the two types of AgNP surfaces were different in number and entity but similar in their interaction with the Ag<sup>0</sup> core. This occurred through, namely Ag<sup>0</sup>-S, Ag<sup>0</sup>-N, and protein-protein interactions that additionally stabilized the AgNPs and likely played a significant role in directing NPs to bacterial activity, uptake, and bacterial cell receptors. The AgNP-FU were more active against *E. coli*, likely because of the protein types that distinguish them chemically. All these results are corresponding to other studies reported in the literature. Capping agents on AgNP surfaces can be engineered using different proteins, carbohydrates, polymers, or specially designed compounds to ensure that the tailored nanoparticle is most effective against *E. coli*. For example, biogenic AgNP-OR were obtained and able to inhibit *Xanthomonas axonopodis* pv. *citri* growth, even at a low concentration [3]. Similar to *Xanthomonas axonopodis* pv. *citri*, *E. coli* sp. are flagellated

Gram-negative bacteria and AgNPs are known to be highly effective against Gram-negative, multidrug-resistant bacteria [25]. Basu et al. [30] suggested that the coating around the biogenic nanoparticles makes them functionally efficient for biomedical uses, such as the easy adsorption and/or delivery of DNA or hydrophobic drugs. These authors found the protein bands at the 116 kDa and 40 kDa bound to the AgNPs synthesized using *Tricholoma crassum*. They suggested that this protein coating promoted the stability of the NPs in colloid and their catalytic activity. Unfortunately, no information was included regarding the nature of the proteins coating the AgNPs. Jalal et al. [31] used a supernatant of *Candida albicans* for the biosynthesis of AgNPs. They reported a capping layer of protein around the periphery of the NPs, which they suggested was closely related to the production of aberrant morphological structure and severe damage of *Candida albicans* cells by the complete or localized separation of the membrane from the cell wall and membrane. This type of damage has been reported previously to be associated with the capability of the capped AgNPs to anchor to cells at several sites and penetrate inside the cells, which results in cell lysis [32]. The same effect has been reported by other authors and suggested to be related to the production and accumulation of reactive oxygen species inside the cells, which leads to cell death through mitochondrial dysfunctional apoptosis, the release of cytochrome C, nuclear fragmentation, DNA damage, and the activation of caspases [33].

Based on the observed AgNP activities against *E. coli*, the protein capping greatly improves AgNP antibacterial properties, probably by enabling their anchoring to the bacterial membranes, thus initiating membrane reorganization. Bacteria such as *E. coli* have negative electrochemical potential and might repel with the also negative AgNPs. The collision and interaction with the Ag(0) are one of the first events observed and then, the oxidation and chemical bonding of membrane biomolecules (*E. coli*) through Ag(I) is expected to occur. There were observed differences among proteins in the two types of AgNPs, with many oxidoreductases present in AgNP-FU, which contributed to their greater antibacterial activity.

### 3. Methodology

#### 3.1. Materials

Silver nitrate was obtained from Labsynth (Diadema, Brazil) and used without any further purification. Orange peel was obtained from a local canteen (Campinas, Brazil). Hesperidin and cellulose nanofibers were extracted from the orange peel (see the following section). A fungal strain of *Fusarium oxysporum* (strain 551) was provided by the Genetic and Molecular Biology Laboratory, ESALQ-USP (Piracicaba, Brazil).

#### 3.2. Biogenic AgNP Synthesis and Characterization

The synthesis of biogenic silver nanoparticles (AgNPs) was performed using three different methods already described in the literature [3,8,12]. Fungal-filtrate-based AgNPs were prepared from a culture of *Fusarium oxysporum*, which was grown for one week in a solid culture medium (0.5% yeast extract, 2% malt, 2% agar, and distilled water) at 28 °C. The fungal culture was then transferred into sterile distilled water and maintained under constant stirring for 72 h until the filtrate reached a protein concentration of 0.1 g mL<sup>-1</sup>. The fungal extract was filtered, and then 0.001 mol L<sup>-1</sup> of AgNO<sub>3</sub> was added to the protein-rich supernatant. The final concentration of Ag(I) ions in the colloid was 5 × 10<sup>-4</sup> mol L<sup>-1</sup>. The mixture was kept protected from light at 28 °C for 96 h until silver nanoparticles formed. The AgNPs synthesized using this methodology were labeled AgNP-FU [8].

The second type of biogenic silver nanoparticles was synthesized from orange peel extract. The extract was prepared using 50 g of orange peels mixed in 800 mL of sterile distilled water. The mixture was heated to a boil and kept boiling for 3 min. The resulting suspension was filtered using a 0.22 µm pore membrane filter, and then 1 mmol L<sup>-1</sup> of AgNO<sub>3</sub> was added to the orange peel extract in a ratio of 1:1 (v/v) to the final concentration of 5 × 10<sup>-4</sup> mol L<sup>-1</sup>. The filtrate was kept in the dark for 48 h. The AgNPs synthesized using this methodology were labeled AgNP-OR [3].

The third type of biogenic silver nanoparticles was synthesized using hesperidin and cellulose nanofibers obtained from orange peels and labeled AgNP Hsp-CNF. Hesperidin was extracted from oven-dried orange peels (68 g), which were inserted in a Soxhlet cartridge extractor apparatus and treated for 1.5 h with 500 mL of diethyl ether to eliminate lipids. Then, the orange peels were treated with 500 mL for 4 h to extract the hesperidin. The solvent was evaporated, and the hesperidin was precipitated by adding 150 mL of 6% acetic acid solution. The precipitate was filtered using a Büchner funnel and rinsed with distilled water. The yellow solid was recrystallized from the dimethyl sulfoxide (DMSO, 16 mL) solution at 60 °C. Cellulose nanofibers (CNF) were produced according to a previously published procedure [13]. For AgNP synthesis, the CNF suspension was made by suspending 0.01% CNF in water and sonicating the mixture for 10 min. The CNF suspension was mixed at a 1:1 (*v/v*) ratio with 1 mmol L<sup>-1</sup> AgNO<sub>3</sub>, and then the mixture was placed in an ultrasonic bath for 15 min. Hesperidin solution (2.0 mg mL<sup>-1</sup> in 1 mol L<sup>-1</sup> NaOH) was then added to a final 1:2:2 *v/v/v* (hesperidin/CNF/AgNO<sub>3</sub>), while stirring, to the resulting suspension after sonication [3]. Silver nanoparticles were obtained after 2 h.

### 3.3. Zeta Potential and Dynamic Light Scattering

The average size, polydispersity, and zeta potential of the different AgNPs (e.g., AgNP-FU, AgNP-OR, and AgNP Hsp-CNF) were determined using dynamic light scattering (DLS) on a Zetasizer Nano ZS (Malvern Instruments Corp., Malvern, UK) laser. All analyses were performed at 25 °C using a disposable folded capillary cell DTS1070 and running three measurements with 15 scans each in triplicate.

### 3.4. Transmission Electron Microscopy

The surface morphology of the synthesized AgNP samples was characterized using transmission electron microscopy (TEM, Carl-Zeiss Libra 120, Jena, Germany). The nanoparticle suspensions were diluted in deionized water to a ratio of 1:3 (*v/v*) and dried overnight on the carbon-coated films. The TEM analyses were performed in a vacuum while applying 80 kV.

### 3.5. Mass Spectrometry

Proteomic analyses were performed at the Brazilian Biosciences National Laboratory (LNBio) of the Brazilian Center for Research in Energy and Materials (CNPEM) (Campinas, Brazil). The protein-capped silver nanoparticles (AgNP-FU and AgNP-OR) were analyzed after trypsin (Sequencing Grade Modified Trypsin, Promega, Sao Paulo, Brazil) lysis using the protocol described in [8] and [3]. Peptides were isolated using Oasis HLB (Waters, Milford, CT, USA) solid-phase extraction (SPE) cartridges with a 1 mL capacity and C18 filling and then concentrated in a SpeedVac (Thermo Scientific, Waltham, MA, USA). The samples were dissolved into 8 µL of water containing 0.1% formic acid (*v/v*), centrifuged, and then the supernatant was transferred to vials and submitted to liquid chromatography/mass spectrometry (LC-MS/MS) analysis. The LC-MS/MS analysis was performed using an RP-nanoUPLC (nanoAcquity, Waters, Milford, USA) with a C18 column (100 mm × 6100 mm) loaded with 4.5 µL of the sample. The Q-ToF Premier mass spectrometer was operated with a nanoelectrospray source at a flow rate of 0.6 mL min<sup>-1</sup> using a gradient of 2–90% acetonitrile with 0.1% formic acid (*v/v*) as a mobile phase for 90 min. A nanoelectrospray voltage value of 3.5 kV, cone voltage of 30 V, and supply the temperature of 100 °C were applied. The LC-MS/MS analysis was performed in MS/MS fragmentation and the ion was blacklisted by 60 s [10]. Finally, the spectra were analyzed using MassLynx v.4.1 software, the files were converted to a peak list format (mgf) without adding the scans by Mascot Distiller v.2.3.2.0, 2009 software (Matrix Science, Ltd., London, UK). The search protein was made using the MS data banks for fungal protein identification, CitrusSinensis2017 database (8814936207566 residues), and Mascot Engine v.2.3.01 (Matrix Science, Ltd., London, UK). Carbamidomethylation was used as the fixed modification and the methionine residue oxidation was used as the variable modification, and then the lost

trypsin cleavage and tolerance of 0.1 Da for both the precursor ion and fragments were determined. In addition to the protein identification provided by Mascot Engine v.2.3.01, ion scores above 10 were manually aligned using the NCBI's Basic Local Alignment Search Tool (Protein BLAST, Center for Biotechnology Information) using sequences of nonredundant proteins of organisms from the *Citrus* genus (taxid: 2706). Only proteins with 100% identity and coverage of the submitted peptide sequence [12].

### 3.6. *Escherichia coli* Inactivation Tests

#### 3.6.1. Bacterial Strain Culture

The bacterial strain used to study the inactivation effects of biogenic silver nanoparticles (AgNPs) was *E. coli* (ATCC 25922) acquired from the UDLAP microbial collection. The *E. coli* strains were kept frozen at  $-80\text{ }^{\circ}\text{C}$  in tryptic soy broth (Bioxon<sup>®</sup>) with 20% of glycerol. From the frozen stock, *E. coli* cells were cultured on MacConkey agar (Bioxon<sup>®</sup>) to verify the corresponding colony morphology. Later, *E. coli* cells were grown on solid nutrient agar (Bioxon<sup>®</sup>) culture media. Cells were collected from an overnight plate culture incubated at  $37\text{ }^{\circ}\text{C}$  under aerobic conditions, centrifuged, rinsed three times with a sterile physiological solution (0.85% NaCl), and adjusted with the same solution using the McFarland standard to obtain an initial concentration of  $10^8$  colony forming units (CFU) per milliliter.

#### 3.6.2. Bacterial Inactivation Tests

We used  $0.1\text{ }\mu\text{g mL}^{-1}$  of the different silver nanoparticles (e.g., AgNP-FU, AgNP-OR, or AgNP Hsp-CNF) placed in a glass beaker with 10 mL of distilled water and constantly stirred on a magnetic plate. Before starting the bacterial inactivation tests, the system was sterilized using a UV disinfection lamp ( $\lambda = 260\text{ nm}$ ) in a type II sterile guard hood for 20 min to eliminate any possible bacterial contamination. After sterilization, an inoculum (0.1 mL) of *E. coli* was added to the glass beaker to obtain an initial bacterium concentration of  $\sim 10^6\text{ CFU mL}^{-1}$ . For experiments testing the effect of UV radiation, the system was irradiated with UV radiation ( $\lambda_{\text{max}} = 364\text{ nm}$ ) at 20 cm ( $7136\text{ }\mu\text{W cm}^{-2}$ ) using a 100 W longwave mercury spot lamp (Analytik Jena, Jena, Germany). The temperature of the reaction mixture was controlled at  $20\text{ }^{\circ}\text{C}$  using a thermostatic bath (Polystat, Cole-Parmer, Vernon Hills, USA). The overall system was placed in a closed box to avoid the effects of any other natural or artificial radiation sources. The controlling conditions, UV radiation in absence of the AgNPs, and using the silver nanoparticles (e.g., AgNP-FU, AgNP-OR, or AgNP Hsp-CNN) without UV radiation were also tested. In all the cases, 0.1 mL samples were collected at different times (0, 5, 10, 15, 20, 25, 30, 60, 90, and 120 min) and immediately analyzed for the concentration of remnant bacteria. Every sample was diluted by multiples of ten in the  $10^{-1}$ – $10^{-3}$  range. An aliquot of  $10\text{ }\mu\text{L}$  from each dilution was dropped on a nutrient agar solid culture media plate divided into squares of  $1.2\text{ cm}^2$  and cultured overnight at  $35\text{ }^{\circ}\text{C}$ . Colony-forming units were counted for every dilution to obtain the number of bacteria survivors per volume unit. Since the number of cells was not always the same, calculation adjustments of the proportion of cells were made by dividing the final number of cells by the initial number of cells ( $C/C_0$ ). All experiments were performed in triplicate.

## 4. Conclusions

This paper assesses the potential of three types of biogenic silver nanoparticles (AgNPs) to inactivate *E. coli*, their synergic effects with UV radiation, and their possible use for water disinfection. The synthetic methodology allowed us to obtain AgNPs through green processes that are cheap, easy to follow, and reproducible. In all cases, water was the only solvent that was used to obtain the fungal and plant extracts or plant-derived biomolecules (hesperidin and cellulose nanofibers) for  $\text{Ag}^0$  production and AgNP stabilization. All synthesized AgNPs showed negative zeta potentials, spherical shape, medium size, and similar polydispersity and stabilities. The synthesized AgNPs showed two main types of coatings: (1) fungal secretome (AgNP-FU) or orange's peel proteins (AgNP-OR), and

(2) cellulose nanofibers, i.e., carbohydrates (AgNP Hsp-CNF). The coatings of the different AgNPs were found to significantly influence their anti-*E. coli* activity, with protein-coated NPs being more active than cellulose-nanofiber-coated NPs. Inactivation of *E. coli* in water using UV ( $\lambda = 364$  nm) radiation was found to enhance the activity of protein-capped AgNPs, especially in the case of AgNP-OR. The disinfection efficiency and synergistic benefits of nanoparticles with protein-core coatings and enteric bacteria suggest that this method could improve the efficiency and reliability of water disinfection. A very low dose of the biogenic silver nanoparticles (e.g., up to a quarter fold lower), compared with the literature available on nanomaterials for water disinfection purposes, was capable of almost completely inactivating *E. coli* in water. Therefore, from the experimental results achieved, the AgNP-FU/UV system is the most suitable for use in water disinfection processes to reduce environmental impacts.

**Supplementary Materials:** The following supporting information can be downloaded at: <https://www.mdpi.com/article/10.3390/catal12040430/s1>, Table S1: Analysis of capping proteins of biogenic silver nanoparticles using UPLC-MS/MS, shotgun techniques, and identified using the protein BLAST server (NCBI, <https://blast.ncbi.nlm.nih.gov>, accessed on 7 October 2021)) [8].

**Author Contributions:** Conceptualization, E.R.B. and L.T.; methodology, E.R.B., C.H.N.B., D.S. and L.T.; formal analysis, C.H.N.B. and D.S.; investigation, C.H.N.B., D.S. and L.K.C.; writing, E.R.B., L.T. and D.S.; supervision, project administration, and funding acquisition, L.T. All authors have read and agreed to the published version of the manuscript.

**Funding:** This research was funded by the National Institute for Bioanalytics (INCT Bio) in a joint project from Fundação de Amparo à Pesquisa do Estado de São Paulo (FAPESP, Sao Paulo, Brazil, N° 2014/50867-3), and the Conselho Nacional de Desenvolvimento Científico e Tecnológico (CNPq, Brasilia, Brazil, N° 465389/2014-7). The APC was sponsored by UNICAMP (FUNCAMP, Grant number #5801).

**Data Availability Statement:** The data that support the findings of this study are available on request from the corresponding author, L.T.

**Acknowledgments:** The Brazilian Biosciences National Laboratory—LNBio of the Brazilian Center for Research in Energy and Materials—CNPEM (Campinas, Brazil) is kindly acknowledged, where the proteomic mass spectrometry analyses were performed. We are very grateful for the technical assistance of Daniela Pott Ballottin, Estela Bocarando-Salcido, and Jose Luis Sanchez-Salas. The authors are also grateful to Nicole Damon (DRI) for her editorial review.

**Conflicts of Interest:** The authors declare no conflict of interest.

## References

1. Shannon, M.A.; Bohn, P.W.; Elimelech, M.; Georgiadis, J.G.; Marias, B.J.; Mayes, A.M. Science and technology for water purification in the coming decades. *Nature* **2008**, *452*, 301–310. [[CrossRef](#)] [[PubMed](#)]
2. Villaseñor-Basulto, D.L.; Pedavoah, M.; Bandala, E.R. Plant materials for the synthesis of nanomaterials: Greener Sources. In *Handbook of Ecomaterials*; Martinez, L., Kharissova, O., Kharisov, B.I., Eds.; Springer: Cham, Switzerland, 2018.
3. de Barros, C.H.N.; Cruz, G.C.F.; Mayrink, W.; Tasic, L. Bio-based synthesis of silver nanoparticles from orange waste: Effects of distinct biomolecule coatings on size, morphology, and antimicrobial activity. *Nanotechnol. Sci. Appl.* **2018**, *11*, 1–14. [[CrossRef](#)] [[PubMed](#)]
4. Ali, I.; Peng, C.; Khan, Z.M.; Naz, I.; Sultan, M.; Ali, M.; Abbasi, I.A.; Islam, T.; Ye, T. Overview of microbes based fabricated biogenic nanoparticles for water and wastewater treatment. *J. Environ. Manag.* **2019**, *230*, 128–150. [[CrossRef](#)] [[PubMed](#)]
5. Rolim, W.R.; Pelegrino, M.T.; de Araújo Lima, B.; Ferraz, L.S.; Costa, F.N.; Bernardes, J.S.; Rodrigues, T.; Brocchi, M.; Seabra, A.B. Green tea extract mediated biogenic synthesis of silver nanoparticles: Characterization, cytotoxicity evaluation and antibacterial activity. *Appl. Surf. Sci.* **2019**, *463*, 66–74. [[CrossRef](#)]
6. Santos, L.M.; Stanisic, D.; Menezes, U.J.; Mendonça, M.A.; Barral, T.D.; Seyffert, N.; Azevedo, V.; Durán, N.; Meyer, R.; Tasic, L.; et al. Biogenic silver nanoparticles as a post-surgical treatment for *Corynebacterium pseudotuberculosis* infection in small ruminants. *Front. Microbiol.* **2019**, *10*, 1–11. [[CrossRef](#)] [[PubMed](#)]

7. Sintubin, L.; De Gussem, B.; Van der Meeren, P.; Pycke, B.F.G.; Verstraete, W.; Boon, N. The antibacterial activity of biogenic silver and its mode of action. *Appl. Microbiol.* **2011**, *91*, 153–162. [[CrossRef](#)]
8. Ballotin, D.; Fulaz, S.; Souza, M.L.; Corio, P.; Rodrigues, A.G.; Souza, A.O.; Marcato, P.G.; Gomes, A.F.; Gozzo, F.; Tasic, L. Elucidating protein involvement in the stabilization of the biogenic silver nanoparticles. *Nanoscale Res. Lett.* **2016**, *11*, 313. [[CrossRef](#)]
9. Huesca-Espitia, L.C.; Auriolés-López, V.; Ramírez, I.; Sánchez-Salas, J.L.; Bandala, E.R. Photocatalytic inactivation of highly resistant microorganisms in water: A kinetic approach. *J. Photochem. Photobiol. A Chem.* **2017**, *337*, 132–139. [[CrossRef](#)]
10. Rahman, A.U.; Khan, A.U.; Yuan, Q.; Wei, Y.; Ahmad, A.; Ullah, S.; Khan, Z.U.H.; Shams, S.; Tariq, M.; Ahmad, W. Tuber extract of *Arisaema flavum* eco-benignly and effectively synthesizes silver nanoparticles: Photocatalytic and antibacterial response against multidrug resistant engineered *E. coli* QH4. *J. Photochem. Photobiol. B Biol.* **2019**, *193*, 31–38. [[CrossRef](#)]
11. Xu, X.; Wang, S.; Yu, X.; Dawa, J.; Gui, D.; Tang, R. Biosynthesis of Ag deposited phosphorus and sulfur co-doped g-C<sub>3</sub>N<sub>4</sub> with enhanced photocatalytic inactivation performance under visible light. *Appl. Surf. Sci.* **2020**, *50*, 144245. [[CrossRef](#)]
12. Mariño, M.; Da Silva, L.L.; Durán, N.; Tasic, L. Enhanced materials from nature: Nanocellulose from citrus waste. *Molecules* **2015**, *20*, 5908–5923. [[CrossRef](#)] [[PubMed](#)]
13. Agrossott, E.V.; Blatte, D.; Cunha, F.A.; Noronha, V.T.; Ciesielski, R.; Hartschuh, A.; Paula, A.J.; Fachine, P.B.; Souza Filho, A.G.; Paschoal, A.R. Vibrational spectroscopy and morphological studies on protein-capped biosynthesized silver nanoparticles. *ACS Omega* **2020**, *5*, 386–393. [[CrossRef](#)] [[PubMed](#)]
14. Alothman, M.; Abeer, A. Effect of green synthesis silver nanoparticles from five fruits peel on protein capped and anti-fungal properties. *Int. J. Adv. Res. Biol. Sci.* **2019**, *6*, 156–165.
15. Xu, Q.; Jin, L.; Wang, Y.; Chen, H.; Qin, M. Synthesis of silver nanoparticles using dialdehyde cellulose nanocrystal as a multi-functional agent and application to antibacterial paper. *Cellulose* **2019**, *26*, 1309–1321. [[CrossRef](#)]
16. Abdel-Raouf, N.; Al-Enazi, N.M.; Ibraheem, I.B.M.; Alharbi, R.M.; Alkhulaifi, M.M. Biosynthesis of silver nanoparticles by using of the marine brown alga *Padina pavonia* and their characterization. *Saudi J. Biol. Sci.* **2019**, *26*, 1207–1215. [[CrossRef](#)]
17. Phan, D.N.; Dorjgudger, N.; Khan, M.Q.; Saito, Y.; Taguchi, G.; Lee, H.; Mukai, Y.; Kim, I.S. Synthesis and attachment of silver and copper nanoparticles on cellulose nanofibers and comparative antibacterial study. *Cellulose* **2019**, *26*, 6629–6640. [[CrossRef](#)]
18. Wahab, J.A.; Kim, I.S.; Ni, Q. Cellulose acetate nanofibers embedded with AgNPs anchored TiO<sub>2</sub> nanoparticles for long term excellent antibacterial applications. *Carbohydr. Polym.* **2019**, *207*, 640–649.
19. Osman, G.; Mohamed, M.M.; Khairou, K.S. Photocatalytic bacterial disinfection using Ag<sup>0</sup>/Ag<sup>1+</sup> immobilized on CNT modified TiO<sub>2</sub> nanomaterials. *J. Pure Appl. Microbiol.* **2019**, *13*, 767–778. [[CrossRef](#)]
20. Ravichandran, V.; Vasanthi, S.; Shalini, S.; Shah, S.A.A.; Tripathy, M.; Paliwal, N. Green synthesis, characterization, antibacterial, antioxidant and photocatalytic activity of *Parkia speciosa* leaves extract mediated silver nanoparticles. *Results Phys.* **2019**, *15*, 102565. [[CrossRef](#)]
21. Castillo-Ledezma, J.H.; López-Malo, A.; Pelaez, M.; Dionysiou, D.D.; Bandala, E.R. Modeling the enhanced photocatalytic solar disinfection of *Escherichia coli* using nitrogen-doped TiO<sub>2</sub>. *J. Surfaces Interfaces Mater.* **2014**, *2*, 334–342. [[CrossRef](#)]
22. Isik, T.; Elhousseini Hilal, M.; Horzum, N. Green synthesis of zinc oxide nanostructures. In *Zinc Oxide Based Nanomaterials and Devices*; IntechOpen: Rijeka, Croatia, 2019.
23. Ramírez-Sánchez, I.; Bandala, E. Photocatalytic degradation of estriol using iron-doped TiO<sub>2</sub> under high and low UV irradiation. *Catalysts* **2018**, *8*, 625. [[CrossRef](#)]
24. Thatikayala, D.; Jayarambabu, N.; Banothu, V.; Ballipalli, C.B.; Park, J.; Rao, K.V. Biogenic synthesis of silver nanoparticles mediated by *Theobroma cacao* extract: Enhanced antibacterial and photocatalytic activities. *J. Mater. Sci. Mater. Electron.* **2019**, *30*, 17303–17313. [[CrossRef](#)]
25. Iqbal, M.; Raja, N.I.; Mashwani, Z.; Wattoo, F.H.; Hussain, M.; Ejaz, M. Assessment of green synthesized silver nanoparticles in wheat seedlings at the anatomical level in relation to their uptake, translocation, and accumulation. *Iran J. Sci. Technol.* **2019**, *43*, 1551–1561. [[CrossRef](#)]
26. Raota, C.S.; Cerbaro, A.F.; Slvador, M.; Delamare, A.P.L.; Echeverrigaray, S.; Crespo, J.S.; da Silva, T.B.; Giovanela, M. Green synthesis of silver nanoparticles using an extract of Ives cultivar (*Vitis labrusca*) pomace: Characterization and application in wastewater disinfection. *J. Environ. Chem. Eng.* **2019**, *7*, 103383. [[CrossRef](#)]
27. He, J.; Zeng, X.; Lan, S.; Lo, I.M. Reusable magnetic Ag/Fe, N-TiO<sub>2</sub>/Fe<sub>3</sub>O<sub>4</sub>@SiO<sub>2</sub> composite for simultaneous photocatalytic disinfection of *E. coli* and degradation of bisphenol A in sewage under visible light. *Chemosphere* **2019**, *217*, 869–878. [[CrossRef](#)] [[PubMed](#)]
28. Sreeja, S.; Vidya Sheets, K. Microbial disinfection of water with endotoxin degradation by photocatalysis using Ag@TiO<sub>2</sub> core shell nanoparticles. *Environ. Sci. Pollut. Res.* **2016**, *23*, 18154–18164.
29. Gnanadhas, D.P.; Ben Thomas, M.; Thomas, R.; Raichur, A.M.; Chakravorty, D. Interaction of silver nanoparticles with serum proteins affects their antimicrobial activity in vivo. *Antimicrob. Agents Chemother.* **2013**, *57*, 4945–4955. [[CrossRef](#)]

30. Basu, A.; Ray, S.; Chowdhury, S.; Sarkar, A.; Mandal, D.P.; Bhattacharjee, S.; Kundu, S. Evaluating the antimicrobial, apoptotic, and cancer cell gene delivery properties of protein-capped gold nanoparticles synthesized from the edible mycorrhizal fungus *Tricholoma crassum*. *Nanoscale Res. Lett.* **2018**, *13*, 154. [[CrossRef](#)]
31. Jalal, M.; Ansari, M.A.; Alzohairy, M.A.; Ali, S.G.; Khan, H.M.; Almatroudi, A.; Raees, K. Biosynthesis of silver nanoparticles from oropharyngeal candida glabrata isolates and their antimicrobial activity against clinical strains of bacteria and fungi. *Nanomaterials* **2018**, *8*, 586. [[CrossRef](#)]
32. Nasrollahi, A.; Pourshamsian, K.; Mansourkiaee, P. Antifungal activity of silver nanoparticles on some fungi. *Int. J. Nano Dimens.* **2011**, *1*, 233–239.
33. Kim, K.J.; Sung, W.S.; Suh, B.K.; Moon, S.K.; Choi, J.S.; Kim, J.G.; Lee, D.G. Antifungal activity and mode of action of silver nano-particles on *Candida albicans*. *BioMetals* **2009**, *22*, 235–242. [[CrossRef](#)] [[PubMed](#)]